

 Open access • Journal Article • DOI:10.1017/RDC.2019.116

Onset of the Younger Dryas Recorded with ^{14}C at Annual Resolution in French Subfossil Trees — [Source link](#)

Manuela Capano, Cécile Miramont, Lisa Shindo, Frédéric Guibal ...+4 more authors

Institutions: Aix-Marseille University, Heidelberg University

Published on: 03 Aug 2020 - Radiocarbon (Cambridge University Press (CUP))

Topics: Younger Dryas, Subfossil and Allerød oscillation

Related papers:

- [IntCal13 and Marine13 radiocarbon age calibration curves 0-50,000 years cal BP](#)
- [A signature of cosmic-ray increase in ad 774–775 from tree rings in Japan](#)
- [Atmospheric \$^{14}\text{C}/^{12}\text{C}\$ changes during the last glacial period from Hulu Cave.](#)
- [Lateglacial and early-Holocene climate variability reconstructed from multi-proxy records on Andøya, northern Norway](#)
- [Another rapid event in the carbon-14 content of tree rings](#)

Share this paper:    

View more about this paper here: <https://typeset.io/papers/onset-of-the-younger-dryas-recorded-with-14c-at-annual-2nk4oe1cgq>



HAL
open science

Onset of the Younger Dryas Recorded with 14 C at Annual Resolution in French Subfossil Trees

Manuela Capano, Cécile Miramont, Lisa Shindo, Frédéric Guibal, Christian Marschal, Bernd Kromer, Thibaut Tuna, Edouard Bard

► **To cite this version:**

Manuela Capano, Cécile Miramont, Lisa Shindo, Frédéric Guibal, Christian Marschal, et al.. Onset of the Younger Dryas Recorded with 14 C at Annual Resolution in French Subfossil Trees. Radiocarbon, University of Arizona, 2020, 62 (4), pp.901-918. 10.1017/RDC.2019.116 . hal-03048599

HAL Id: hal-03048599

<https://hal-amu.archives-ouvertes.fr/hal-03048599>

Submitted on 9 Dec 2020


HAL is a multi-disciplinary open access archive for the deposit and dissemination of scientific research documents, whether they are published or not. The documents may come from teaching and research institutions in France or abroad, or from public or private research centers.

L'archive ouverte pluridisciplinaire **HAL**, est destinée au dépôt et à la diffusion de documents scientifiques de niveau recherche, publiés ou non, émanant des établissements d'enseignement et de recherche français ou étrangers, des laboratoires publics ou privés.



Distributed under a Creative Commons Attribution - NonCommercial - NoDerivatives | 4.0 International License

ONSET OF THE YOUNGER DRYAS RECORDED WITH ^{14}C AT ANNUAL RESOLUTION IN FRENCH SUBFOSSIL TREES

Manuela Capano^{1*}  • Cécile Miramont² • Lisa Shindo² • Frédéric Guibal² • Christian Marschal² • Bernd Kromer³ • Thibaut Tuna¹ • Edouard Bard^{1*}

¹CEREGE, Aix Marseille University, CNRS, IRD, INRA, Collège de France, Technopôle de l'Arbois, Aix-en-Provence, France

²Aix Marseille University, Avignon University, CNRS, IRD, IMBE, Marseille, France

³Institute of Environmental Physics, University of Heidelberg, Germany

ABSTRACT. Subfossil trees with their annual rings constitute the most accurate and precise archive to calibrate the radiocarbon (^{14}C) method. The Holocene part of the IntCal curve is based on tree-ring chronologies, absolutely dated by dendrochronological matching. For the Northern Hemisphere, the absolute curve starts at 12,325 cal BP. For the early part of the Younger Dryas (YD) climatic event ($\approx 12,850$ – $11,650$ cal BP), there are only a few floating dendrochronological sequences, mainly from Switzerland and France. We present new ^{14}C results from subfossil trees (*Pinus sylvestris* L.) collected from the Barbières site (southeast French Alps). The dendrochronological series covers 416 years, corresponding to the onset of the YD period. In order to date our sequence, we matched it with the ^{14}C record based on kauri trees from New Zealand. The Barbières data were first averaged at the same decadal resolution as the kauri record. Statistical comparison of the different averaging options and matching techniques enables dating the Barbières sequence to 13,008–12,594 ± 10 cal BP, which thus includes the boundary between the Allerød and YD events. The new Barbières record allows to calculate the ^{14}C inter-hemispheric gradient (^{14}C -IHG) during the period overlapping the kauri sequence. For the optimal dating option, the mean ^{14}C -IHG is 37 yr with a standard deviation (SD) of 21 yr based on 43 decadal estimations (-6% with SD of 2%). The ^{14}C -IHG record exhibits minimal values, down to zero, between 12,960–12,840 cal BP. Excluding these minima leads to an average ^{14}C -IHG of 45 yr with a SD of 14 yr based on 33 decadal values, in agreement with observations for the last two millennia. The Barbières record suggests a ^{14}C -IHG increase between the end of the Allerød period (IHG of 37 yr with SD of 14 yr) and the early part of the YD (IHG of 48 yr with SD of 14 yr), which is compatible with previously reported drop of deep-water convection in the North-Atlantic and the associated increase in wind-driven upwelling in the Southern Ocean.

KEYWORDS: ^{14}C calibration, carbon cycle, dendrochronology, interhemispheric gradient, Younger Dryas.

INTRODUCTION

Radiocarbon (^{14}C) is commonly used to date biogenic samples sourcing from over the past 50,000 yr. While alive, organisms equilibrate their $^{14}\text{C}/^{12}\text{C}$ ratio with that of the atmospheric pool and, when they die, this ratio begins to decrease as ^{14}C decays. The $^{14}\text{C}/^{12}\text{C}$ ratio of a biological sample correlates with the time that has elapsed since its death (Libby 1954). However, the atmospheric $^{14}\text{C}/^{12}\text{C}$ ratio varies through time and space due to fluctuations of ^{14}C production rate (originating mainly via changes in solar activity and/or in geomagnetic field intensity) and to changes in the carbon cycle, making it necessary to correct atmospheric ^{14}C fluctuations in order to calculate accurate ages. For this purpose, a calibration curve is needed, obtained by comparing raw ^{14}C ages with true calendar ages derived from independent dating methods (e.g. Reimer et al. 2013).

Various archives are used to construct the ^{14}C calibration curve, but the best is based on dendrochronologically dated tree-ring series. For the Holocene (\approx the past 11,600 yr), subfossil trees are abundant, allowing the construction of a calibration curve dated absolutely with annual resolution. For times before the Holocene, the availability of trees is limited to some areas and periods (Kaiser et al. 2012). While subfossil trees that lived during warm periods (e.g. Bølling and Allerød phases) are fairly common (Miramont et al. 2010; Kaiser et al. 2012; Adolphi et al. 2017; Reinig et al. 2018), trees corresponding to the Younger Dryas cold phase are exceptional (Miramont et al. 2011). Indeed, the Younger Dryas (YD) gap prevents the Bølling-Allerød floating sequences from being connected with the absolute chronology (Kaiser et al. 2012; Reinig et al. 2018).

* Corresponding authors. Emails: capano@cerge.fr, bard@cerge.fr.

Capano et al. (2018) analyzed ^{14}C in two trees of the Barbiers chronology from the southeast French Alps and reconstructed a continuous 240-yr chronology that was used to tentatively link the absolute calibration curve (Kaiser et al. 2012) with the floating CELM (Central European Lateglacial Master) chronology for the Allerød period. In this follow-up study, we present an augmented 416-yr tree-ring chronology based on five trees from the Barbiers site, annually ^{14}C dated to the onset of the YD period.

The ^{14}C content measured in French subfossil trees is also compared to kauri records from the Southern Hemisphere (Hogg et al. 2016a, 2016b) and employed to study the atmospheric ^{14}C gradient between the Northern and Southern Hemispheres (NH and SH). Indeed, a systematic ^{14}C difference exists between wood from trees that lived at the exact same time in the NH and SH (SH wood being generally older than NH wood). Precise measurement of this ^{14}C interhemispheric gradient (^{14}C -IHG) and its variations over the Allerød-YD transition is of prime interest for identifying changes in the global carbon cycle during the last deglaciation. The chronological accuracy of the tree-ring record allows comparison of the ^{14}C -IHG variations with other carbon cycle changes evidenced in the atmospheric CO_2 and CH_4 records measured in bubbles occluded in polar ice cores over the Late Glacial period (Marcott et al. 2014).

^{14}C Chronologies from Tree Rings over the Younger Dryas Event

The synchronization of the German HOC (Holocene Oak Chronology) and PPC (Preboreal Pine Chronology) sequences gave rise to a long dendrochronological series, starting (i.e. oldest year) at 12,410 cal. BP (Friedrich et al. 2004). This chronology was then extended into the Younger Dryas period with the Swiss YD sequences, leading to an absolute chronology starting at 12,594 cal BP (Schaub et al. 2008; Hua et al. 2009, Kaiser et al. 2012). However, Hogg et al. (2013) highlighted problems in the dendrochronological synchronization of the Ollon505 larch tree with the PPC. Indeed, the ^{14}C data of decadal tree-ring samples from the absolute chronology were included in the IntCal13 calibration curve, but the Ollon505 larch tree was excluded (Reimer et al. 2013).

In the framework of the 2015 IntCal Workshop in Zurich, Michael Friedrich corrected the matching of sequences and validated the chronology up to 12,325 cal BP (Kromer et al. 2015). New dendrochronological and ^{14}C analyses performed in Zurich have been dedicated to filling the gap between the absolute chronology and the YD floating chronologies (Reinig et al. 2018). In addition, floating tree-ring chronologies also exist for the Allerød period: the German LGP (Late Glacial Pine) and the Swiss SWILM (Swiss Late-glacial Master) chronologies, synchronized in the CELM chronology; Italian chronologies from Carmagnola and Avigliana; and French chronologies from the Drouzet site (Kaiser et al. 2012; Adolphi et al. 2017).

For the YD onset, only a few floating chronologies are available for the NH:

- The Barb12-17 sequence, a 240-yr chronology belonging to the French Barbiers chronology that has been sampled at annual resolution for ^{14}C measurements (Capano et al. 2018). Preliminary ^{14}C dating of the Barb12-17 sequence between ca. 12,836 to 12,594 cal BP (Capano et al. 2018) was based on visual matching of wiggles against the kauri sequence from New Zealand (Hogg et al. 2016a, 2016b).
- The youngest part of the CELM chronology, a 1606-yr chronology composed of Swiss and German pines from the Danube (Kaiser et al. 2012). The last ring of the youngest tree of the sequence (G5) has been dated in several works to between ca. 12,500 and $12,844 \pm 32$ cal BP

(Hughen et al. 2000; Muscheler et al. 2008; Hua et al. 2009; Bronk Ramsey et al. 2012; Hogg et al. 2016b; Capano et al. 2018).

- The Swiss YD chronologies. YDB (Younger Dryas B) was the oldest series included in the absolute dendrochronological sequence starting at 12,594 cal BP (Schaub et al. 2008). The ^{14}C measurements have been complemented with measurements at annual resolution of the original YD series and of the new floating Late Glacial subfossil pine chronologies from Zurich, Switzerland, the so-called “Binz” find (Reinig et al. 2018; Sookdeo et al. 2019).

For the SH, the YD period is recorded in two floating chronologies. As is the case for NH records, these chronologies have been dated through ^{14}C measurements:

- The huon pine [*Lagarostrobos franklinii* (Hook.f.) Quinn] chronology from Tasmania (Australia), a floating 617-yr chronology dated through wiggle-matching to ca. 12,760–12,070 cal BP (Hua et al. 2009). The LGP chronology reaching ca. 14,200 cal BP, was linked to the absolute chronology by using the huon pine bridge (Reimer et al. 2013).
- The kauri [*Agathis australis* (D. Don) Steudel] chronology, a 1451-yr floating chronology from Towai (New Zealand), which spans the period between ca. 13,134 and 11,694 cal BP based on the ^{14}C wiggle-matching with the absolute IntCal13 curve overlapping between 11,874 and 11,694 cal BP (Hogg et al. 2016a, 2016b; Reimer et al. 2013). Hogg et al. first revised the dating of the YDB chronology, the beginning of which was positioned at 12,615 cal BP, and then used the kauri chronology to connect the YDB and the CELM sequences, thus extending the tree-ring record back to $14,174 \pm 3$ cal BP (Hogg et al. 2016a, 2016b). Sookdeo et al. (2019) measured ^{14}C at annual to 5-yr resolution in Cottbus and Breintenthal woods over the period 12,324–11,880 cal BP, allowing to recalibrate the kauri sequence over a longer period (i.e. ca. 400 yr), thus refining the dating of the kauri chronology to $13,144\text{--}11,704 \pm 6$ cal BP.

For this new study, we further analyzed the ^{14}C concentration in tree rings of subfossil pines from the French Barbiers chronology, creating an annual-resolution ^{14}C sequence spanning more than 400 yr. Because the new data from Swiss trees are still floating and not yet published, we compare our new record only with chronologies from the SH (Hua et al. 2009; Hogg et al. 2016a, 2016b), allowing to date the Barbiers chronology.

SITE AND MATERIALS

The Barbiers River site (44.354899N, 5.830316E) is located at an altitude of 660 m at the foot of Mount Saint Genis, which culminates at 1260 m in the Middle Durance area (southern French Alps). Several hundred subfossil trees (*Pinus sylvestris* L.) from the Late Glacial and Holocene periods have been discovered there (Miramont et al. 2000; Kaiser et al. 2012), and their noteworthy fossilization and preservation can be explained by a combination of climatic, geologic and topographic factors: (1) this region is submitted to stormy rainfall influenced by both Mediterranean and mountain climates (Frei and Schär 1998; Kieffer-Weisse and Bois 2001); (2) bedrock consists of highly erodible calcareous marl (Gidon et al. 1991); and (3) steep slopes are widely developed in this alpine area.

During the Late Glacial Maximum (LGM) the Durance glacier, which had reached its maximal extent (Jorda et al. 2000), was near the Barbiers River site. A dry and cold climate prevailed and the flanks of Mount Saint Genis were covered by scree slopes. After the LGM, rapid warming accompanied by increased precipitation led to the reactivation of

the hydrological cycle in unglaciated rivers such as Barbiere River. With increased runoff came intense erosion of steep and erodible slopes, leading to silty and coarse riverine sediment deposition, which formed wide and deep alluvial fans, the so-called “Main Postglacial Infilling” (MPI), which dates to 14,500–6,000 cal BP (Miramont et al. 2004). In the Middle Durance area, the MPI resulted in vast and flat plains, which have been used for agriculture since Neolithic times. With the occurrence of high sedimentation rates throughout the building of MPI, many trees were buried (mainly *Pinus sylvestris* L.), which represents Lateglacial and early Holocene pioneer vegetation. These trees have remained well preserved and buried until their recent exposure following the vertical incision of the rivers.

Most of the subfossil trunks discovered in the Middle Durance area are 0.2–2 m high, are still rooted in standing position and are well preserved with pieces of bark remaining. Tree-Ring Width series (TRW) show frequent abrupt growth changes, wedging, and missing rings due to sediment deposition and flooding of the rivers (Sivan et al. 2006). Alluvial sediments gradually buried the stumps while the trees were alive, reducing oxygen exchange between the atmosphere and the root system. Trees that were buried in alluvial deposit survived for several years or several decades after flooding, but formed very narrow growth rings, before dying. Because of high sedimentation rates, these trees failed to develop epitrophic or adventive roots.

At the Barbiere River site, 18 trees were found in 2000 (Miramont et al. 2011). New sampling campaigns performed in autumn 2017 revealed 4 new trees from the Barbiere site, and also permitted the resampling of previously analyzed trees, with better-preserved wood and longer series.

METHODS

Dendrochronological Analysis

Whenever possible, 2 or 3 disks of 5–10-cm thickness were sampled from each subfossil pine: one just above the root to estimate the germination date, and one higher on the stem to avoid reaction wood and to measure TRW. Disks were air-dried and sanded flat using progressively finer sandpaper up to 400 grain size. Standard dendrochronological techniques were employed in chronology development (Fritts 1976; Cook and Kairiukstis 1990). TRW was measured on at least 3 *radii* using a LINTAB measuring system with a precision of 0.01mm and the TSAPWin software (Rinn 1996, 2003).

We observed 2 groups of trees belonging to distinct sediment layers: the older one dates from the Allerød-Younger Dryas transition and the younger one dates to around 10,400 BP on the ¹⁴C plateau. In this study we explore only the first group of trees.

The dendrochronological match of sequences was challenging due to growth anomalies resulting from geomorphological stress. Some trees had grown slowly and produced very narrow rings at the beginning or the end of their life. In addition, we identified several missing rings, thanks to the new 2017 disks taken in the lower part of the trunks that helped improving some TRW series correlations (Table 1).

Previously, 9 trees were grouped into 2 floating sequences BARBA (6 trees) and BARBB (3 trees) (Miramont et al. 2011; Kaiser et al. 2012). On the basis of annual radiocarbon measurements, Capano et al. (2018) revised the position of tree Barb17 in the BARBA

Table 1 Correlation matrix of BARB: overlap, Gleichläufigkeit and t-value (BP and H), respectively for each matching position. In bold: Gleichläufigkeit and t-values above 60 and 4.0 which are usually the respective minima required to accept dendro-match.

Tree/ chronology	Barb30	Barb13	Barb14	Barb4	Barb31	Barb9	Barb12	Barb5	Barb7	Barb17
Barb13	92/ 60/5.3 /3.3									
Barb14	88/ 65 /3.4/3.1	104/ 77/8.4/9.0								
Barb4	71/57/2.3/2.5	87/ 69/4.5 /3.3	156/58/ 4.5/5.1							
Barb31	58/ 70/4.0 /3.3	74/ 68/6.4/4.4	89/ 60/5.9/5.5	89/ 62/5.1 /3.9						
Barb9	ovl<60 yrs	ovl<60 yrs	80/ 70 /3.0/ 5.4	80/ 71/4.1/4.9	79/ 61 /2.7/2.7					
Barb12	ovl<60 yrs	ovl<60 yrs	115/58/3.0/3.0	139/ 71/5.7/5.3	61/ 60 /2.4/2.0	62/57/2.3/1.8				
Barb5	ovl<60 yrs	ovl<60 yrs	86/55/0.0/0.3	95/ 61 /2.9/3.0	ovl<60 yrs	ovl<60 yrs	95/ 65 /3.2/3.4			
Barb7	ovl<60 yrs	ovl<60 yrs	83/55/0.5/0.3	107/48/2.0/1.0	ovl<60 yrs	ovl<60 yrs	131/57/3.8/2.6	92/ 66 /3.9/3.6		
Barb17	ovl<60 yrs	ovl<60 yrs	ovl<60 yrs	ovl<60 yrs	ovl<60 yrs	ovl<60 yrs	126/56/3.5/ 5.1	ovl<60 yrs	79/57/0.6/0.8	
BARB*	92/ 60/4.8/4.1	108/ 70/8.9/6.9	173/ 64/7.1/8.2	180/ 66/7.1/6.6	89/ 61/8.2/6.4	80/ 67/3.8/4.7	210/ 60/6.9/9.4	95/ 74/4.8/4.7	96/ 62/4.1/4.4	126/ 60/3.2/5.1

*Without the corresponding tree.

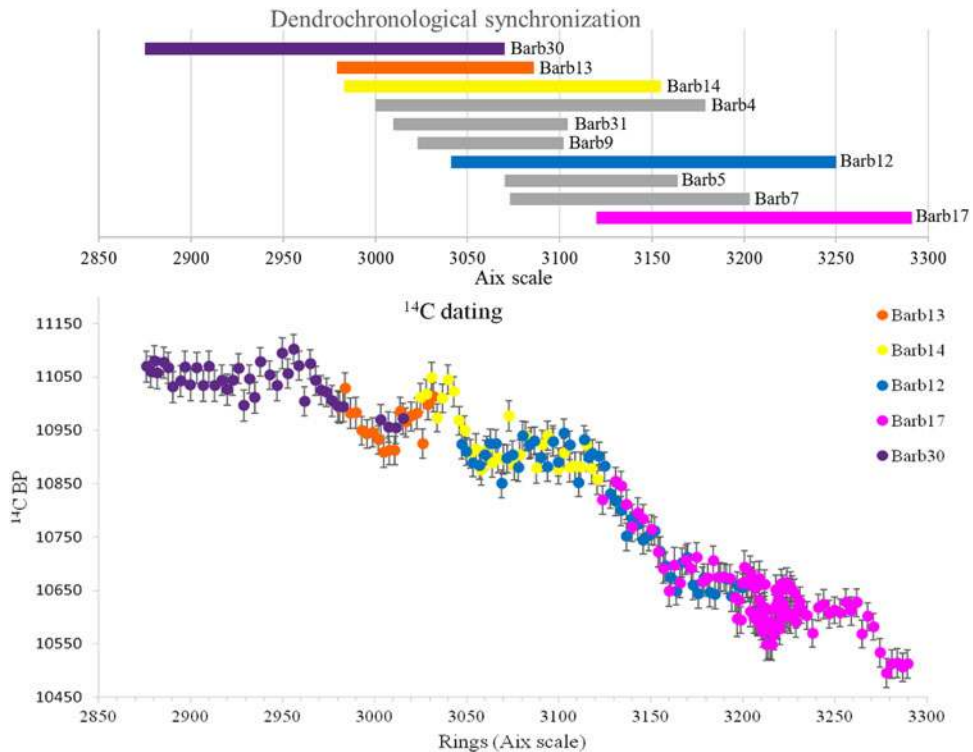


Figure 1 Comparison between the trees included in the Barbiers chronology on the relative Aix scale. The bar diagram of the upper part of the figure reports all cross-dated trees (the gray bars refer to trees that were not ^{14}C dated). In the lower part of the figure, the ^{14}C record for each analyzed tree is shown in its dendrochronological position on the relative Aix scale. (Please see electronic version for color figures.)

chronology. ^{14}C dating confirms the dendro-match between BARBA and BARBB, allowing to merge them in a single chronology BARB (see Figure 1 for the position of the trees composing the BARB chronology). Tree Barb16 has been removed from BARB because the dendro-match is too weak. Trees Barb31 and Barb30 have been added to BARB, thus extending the chronology to 416 yr. The irregular growth of Barb18, Barb32, Barb33, Barb36 and weak correlation coefficients prevent any dendro-matching with the other trees. Table 1 provides the values of the statistical tests (overlap, Gleichläufigkeit and t-value) performed on the different tree sequences grouped in BARB chronology.

Radiocarbon Methods

We analyzed the trees Barb13, Barb14, and Barb30 from the BARB chronology. Clear and mostly regular ring growth in Barb13 and Barb14 allowed systematic sampling of the sequences at annual resolution. Barb30 tree-ring series showed quite different ring patterns. Very narrow rings at the beginning and at the end of the Barb30 sequence led us to mix the wood of 2 rings (3 for sample 1-3) in these parts of the sequence (Table S1).

Sampling was performed on a selection of rings from each tree: rings number #3 to 54 of the 108-yr sequence of Barb13; rings number #43 to 142 of the 173-yr sequence of Barb14; rings number #1 to 155 of the 196-yr sequence of Barb30 (Figure 1; Table S1). Then, every third ring

of the three sequences was measured for ^{14}C . Rings number #72 to 108 of the tree Barb17 were further measured at full annual resolution, with replicated ^{14}C measurements from the same cellulose extracts for rings number #80 to 105. The average absolute value of the differences between 26 replicates pairs is 36 yr with a standard deviation (SD) of 20 yr, which is less than twice the average 1 sigma uncertainty ($2 \cdot 29 = 68$ yr) of these measurements (Table S1). These higher resolution analyses were performed to assess the possible presence of a solar event at around 12,670 cal BP, as hypothesized by Capano et al. (2018).

The wood samples were sliced into small pieces using a scalpel under a binocular microscope, before being treated chemically for cellulose extraction using the ABA-B method. This method consists in a classical ABA treatment, with solutions of HCl and NaOH at 4% concentration, followed by the bleaching step, performed with 60 g of NaClO_2 in 1 L of ultrapure water in acid solution (HCl) at pH 3 (Capano et al. 2018). After chemical pretreatment, the dried residues were weighed in tin capsules, combusted with the elemental analyzer, and the evolved CO_2 was finally transformed into graphite with the AGE III system. The graphite target was then analyzed for its $^{14}\text{C}/^{12}\text{C}$ and $^{13}\text{C}/^{12}\text{C}$ ratios using the AixMICADAS system (Bard et al. 2015). Standards (OxA2 NIST SRM4990c) and blanks (VIRI-K, chemically treated like the other wood samples) were processed together with samples and used for normalization and blank correction, respectively. In addition, IAEA-C3 (cellulose) and IAEA-C8 (oxalic acid) standards were pretreated (IAEA-C3 underwent also the chemical pretreatment) and measured for ^{14}C in the same batches, serving as control standards.

High precision ^{14}C measurements were performed with long AMS runs to reach at least 800,000 ion counts for each OxA2 standard targets on the same magazine. An additional uncertainty of 1.6‰ was propagated in the ^{14}C analytical errors and background correction following the convention described in Capano et al. (2018). The data are reported in terms of conventional ^{14}C age in yr BP and $\Delta^{14}\text{C}$ in ‰, which is the $^{14}\text{C}/^{12}\text{C}$ ratio after correction for fractionation and decay (Stuiver and Polach 1977). In order to certify our high-precision in wood dating, we successfully participated in the International Intercomparison on wood dating organized by ETH (Zurich) in 2017–2018. Indeed, two wood blanks and three wooden sequences, dated to different periods, were annually dated and the results were compared with those of other laboratories (Wacker et al. 2018).

In order to date the Barbiere chronology, we compared it with the available chronologies from the SH: the kauri chronology from New Zealand (Hogg et al. 2016a, 2016b) and the huon pine chronology from Tasmania (Hua et al. 2009). The kauri chronology has two advantages compared to the huon pine sequence: (1) it spans the entire period covered by the Barbiere chronology and (2) it exhibits less scatter than the huon pine record. Moreover, Hogg et al. (2016b) suggested that synchronization problems still persist between the individual trees of the huon record. For these reasons, we did not tune the Barbiere record to the huon pine record, comparing the Barbiere data just with the kauri record. Kauri sequence is dated by ^{14}C wiggle matching against the absolute tree-ring-based part of the calibration curve (Reimer et al. 2013; Hogg et al. 2016a, 2016b). The dating for kauri proposed by Hogg et al. (2016a, 2016b) was shifted by 10 yr towards older ages following Sookdeo et al. (2019).

In Capano et al. (2018), the dating of the Barbiere sequence was a preliminary determination based on a visual match with the kauri chronology (Hogg et al. 2016a, 2016b). For the present study, we used statistical analyses to compare and match the Barbiere and kauri series (i.e. R-cross-correlation coefficient, χ^2 minimization and the Bayesian statistics tool of the OxCal

program). The χ^2 value varies with both the placement year and the ^{14}C -IHG value, allowing χ^2 minimization with both unknown variables (resulting in a surface in 3D plots such as in Figure 4).

In order to compare our annual-resolution data with decadal-average data from kauri, we compared both records by averaging the Barbiers record to mimic the resolution of the kauri record. For each decade, we calculated the weighted average of the Barbiers ^{14}C data included in the studied decade and the weighted error of the ^{14}C data as the uncertainty for the decadal estimate. The starting year is arbitrary when calculating the Barbiers decadal average. We thus considered all possibilities leading to 10 averaged Barbiers curves, which were then compared with the kauri sequence (the first option starting from rings number #1 to 10 in the sequence, while other options differ by one ring numbers #2-11, #3-12 etc.; Figure 2).

RESULTS

Results of ^{14}C Dating of the Barbiers Series

The ^{14}C results for the Barb14 tree confirm its dendrochronological match with the Barb12 series, ^{14}C -dated in Capano et al. (2018; Figure 1). The dendrochronological position of the well-synchronized trees Barb13 and Barb14 is also confirmed with the new ^{14}C results (Figure 1). The ^{14}C dating confirms the dendro-match between Barb30 and BARB, attested by a high correlation coefficient, but short overlap (Table 1). Overall, this confirms the usefulness of considering ^{14}C data at annual resolution for a more precise synchronization of series characterized by the irregular ring growth typical of the YD event (Figure 1).

Optimization of the cross-correlation coefficient between the Barbiers decadal average curves and the kauri decadal curve shows slightly different optimum results, with the highest correlation observed when the Barbiers series starts at 13,008 cal BP with a decadal average starting with rings number #5 to 14 and so forth (Figures 2 and 3). In fact, all 10 options for averaging Barbiers exhibit high R values (>0.9) and we took this 10-yr range as a conservative error on the Barbiers chronology starting at $13,008 \pm 5$ and ending at $12,594 \pm 5$ cal BP (Figure 5).

The 10 decadal average series for Barbiers and the kauri chronology have been used to calculate the χ^2 distance, which is minimum when the Barbiers series starts at 13,008 cal BP (option starting with the rings number #5-14 average; Figures 2 and 4). As for the optimization of the correlation coefficient, we take the 10-yr range of the different decadal averages as a conservative uncertainty for the placement of the Barbiers series: $13,008$ – $12,594 \pm 5$ cal BP (Figure 5). As described below, the χ^2 minimization also provides an optimal value for the IHG.

Finally, we compared the Barbiers and kauri chronologies by means of the Oxcal statistical program (Bronk Ramsey et al. 2001) (Figure 6). The comparison was performed using the OxCal “Delta_R” uniform function (U(-120,120); Bronk Ramsey 2009) in order to account for the IHG. The 10 average options for Barbiers were compared with the kauri chronology, leading to an optimal placement of $13,001$ – $12,586 \pm 6$ Cal BP (2σ error; Table 2). As for the two previous techniques, we kept all 10 possible solutions as they show similar levels of agreement (Table 2). The youngest and oldest years of the 10 dating solutions lead to a range of 20 yr. This allows to date the Barbiers sequence to $13,006$ – $12,591 \pm 10$ cal BP.

The OxCal Offset function also allows to compare the non-averaged series of Barbiers directly with the decadal record of Kauri. This leads to a chronology date of $13,003$ – $12,588 \pm 25$ cal BP

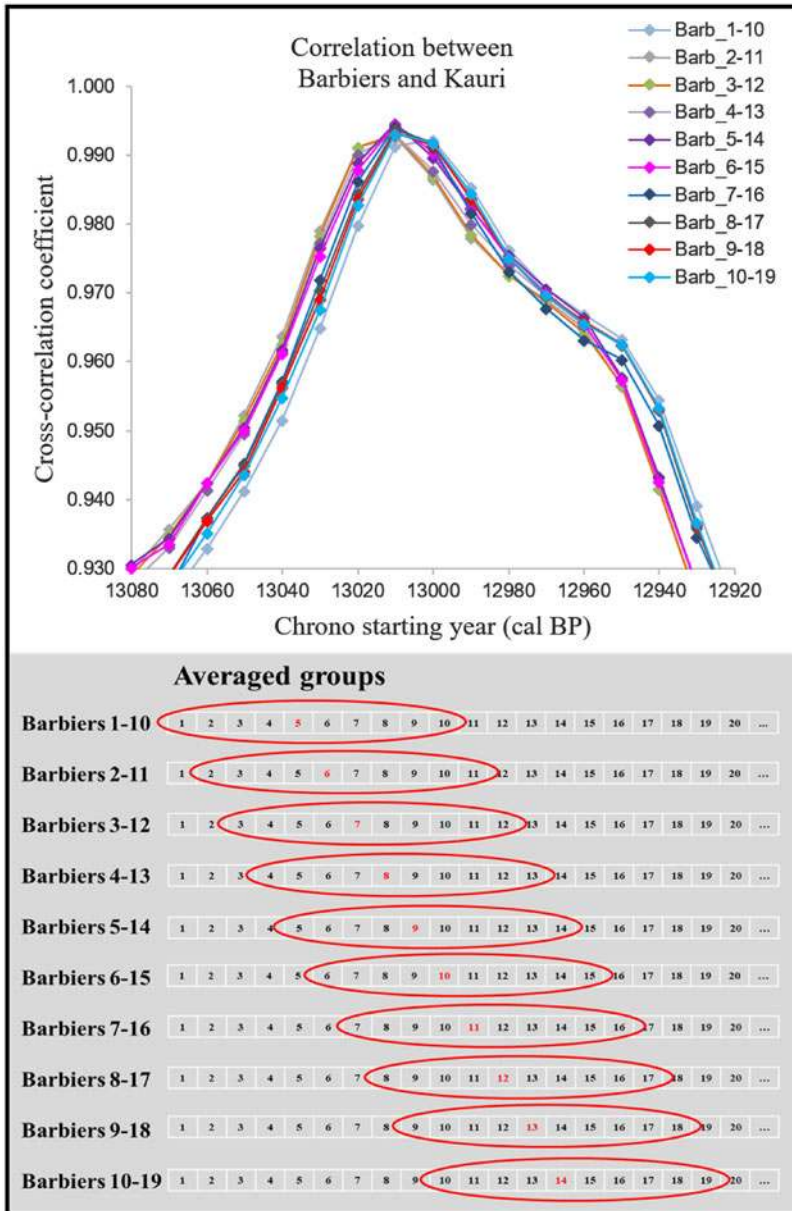


Figure 2 Top: results of the cross-correlation coefficient for the 10 averaged groups of Barbiers series compared against the kauri record. Bottom: the averaging system used for obtaining the 10 groups.

(2σ error range). This dating option agrees with previous estimations, but has a somewhat larger uncertainty, which is linked to the different resolutions of the Barbiers and Kauri datasets.

Overall, the three statistical techniques (cross-correlograms, χ^2 minimization and OxCal Delta_R) provide very similar results for the dating of Barbiers chronology. Taking the

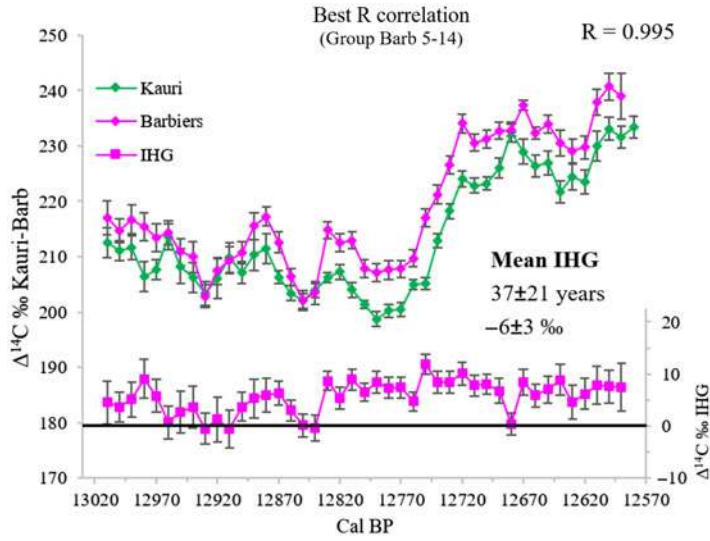


Figure 3 $\Delta^{14}\text{C}$ ‰ of Barbiers averaged groups compared against kauri record. The best dating position of Barbiers chronology obtained from the cross-correlation coefficient is given for each group. The best R value is obtained for the group 5-14. The IHG is shown for all groups compared with kauri (lower part of each graph).

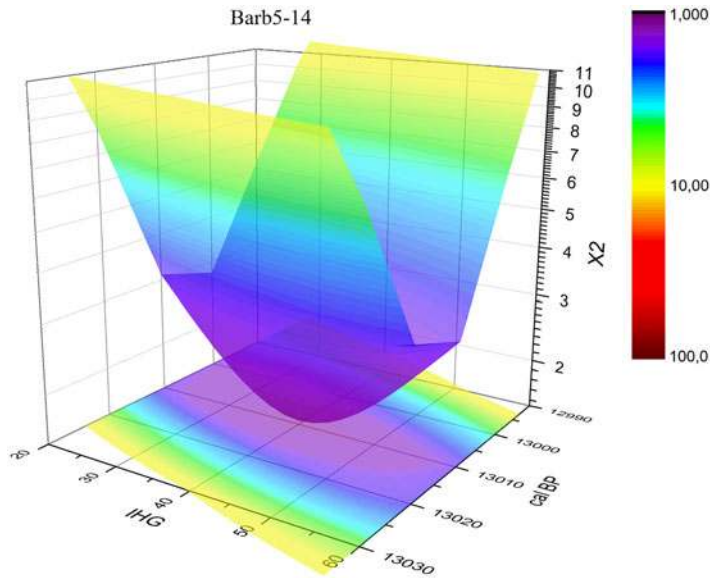


Figure 4 3D representation of the best dating option obtained by comparing Barbiers averaged series with kauri record by means of a χ^2 test. The obtained combination of results suggests that the Barbiers chronology starts at 13,008 cal BP and that the mean IHG value is 40 yr.

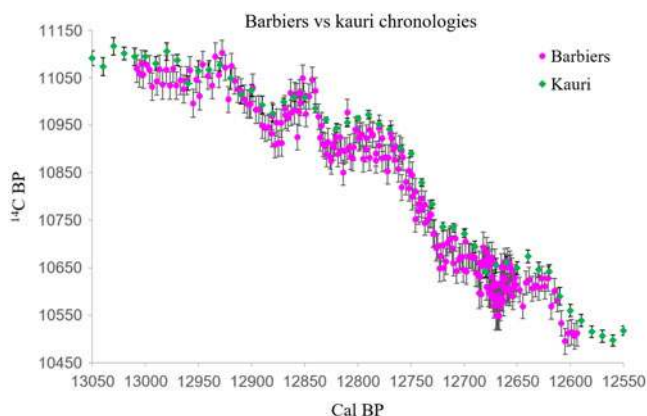


Figure 5 Comparison between the Barbiers and the kauri chronology for the Younger Dryas period. The published kauri chronology (Hogg et al. 2016a, 2016b) is shifted by 10 yr towards older ages (Sookdeo et al. 2019).

largest uncertainty, we can date our sequence to 13,008–12,594 ±10 cal BP. A higher precision for the dating of Barbiers chronology will become possible only when an annual-resolution ^{14}C series of kauri chronology or any other absolutely dated ^{14}C series for the YD period become available.

The existence of a brief $\Delta^{14}\text{C}$ excursion at ca. 12,670 cal BP (12,680 cal BP with the new kauri placement by Sookdeo et al. 2019) was suggested in our previous work (Capano et al. 2018). To evaluate the possibility of a solar event, we have improved the Barbiers ^{14}C record specifically with the Barb17 tree: ^{14}C was measured for every year from rings number #72 to 108 with at least two replicates for rings number #80 to 100 and 102, 105 (Table S1, Figure 1). The high resolution ^{14}C record is characterized by rather noisy ^{14}C values before and during the ^{14}C peak, which makes it difficult to maintain the hypothesis of a sharp solar event.

Results on the Atmospheric ^{14}C IHG

Lerman et al. (1970) were the first to identify the presence of a small but systematic ^{14}C difference between wood from trees that lived at the exact same time in the NH and SH (SH wood being 36 ± 8 yr older than NH wood). This ^{14}C -IHG is maintained principally by air-sea CO_2 exchange with the ocean surface that is typically much older than the atmosphere (from 400 to 1200 yr, Bard 1988). Indeed, there is proportionally more ocean surface in the SH than in the NH, and the Southern Ocean is also characterized by generalized upwelling of old water and intense CO_2 piston velocity due to extreme winds in the 40° to 60°S latitude belt (Levin et al. 1987; Braziunas et al. 1995). The ^{14}C -IHG is even more complex for trees grown after the Industrial Revolution due to anthropogenic fossil CO_2 which has since been emitted mainly in the NH (Stuiver and Braziunas 1998; McCormac et al. 1998), thus disturbing and reversing the gradient.

Following Lerman et al. (1970), several other authors have further quantified the IHG. Hogg et al. (2002) measured the ^{14}C -IHG over the last millennium, deriving an average value of 40 ± 13 yr and suggesting a 130-yr periodicity for ^{14}C -IHG variations. Taking into account the variability of the ^{14}C -IHG, McCormac et al. (2004) proposed using a modeled ^{14}C -IHG

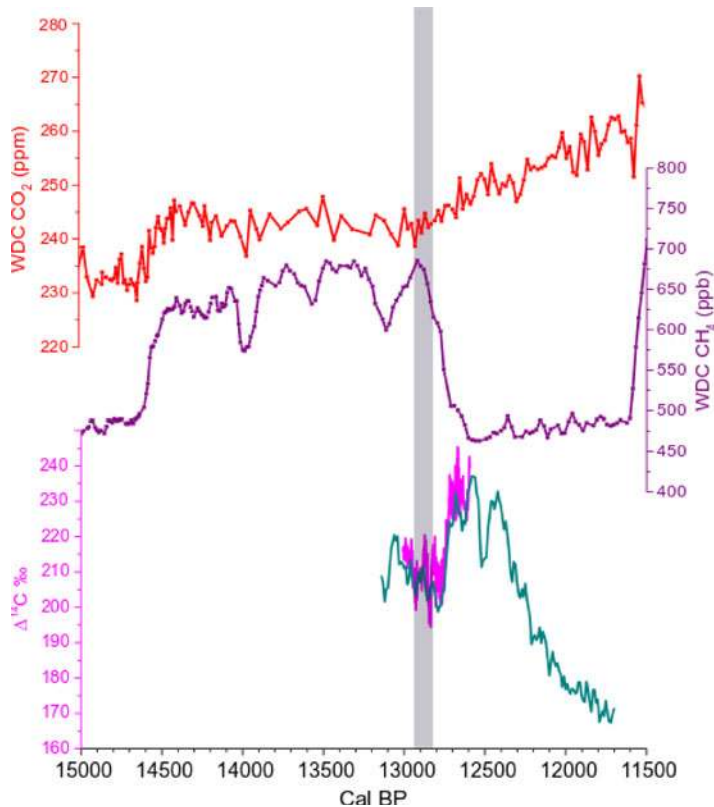


Figure 6 Comparison between Antarctica WDC CO₂ data (red curve, top of graph) on the WD2014 age-scale (Marcott et al. 2014; Buizert et al. 2015), Antarctica WDC CH₄ data (purple curve, middle of graph) on the WD2014 age-scale (Marcott et al. 2014; Buizert et al. 2015), and Δ¹⁴C ‰ from New Zealand kauri trees and French Barbiers trees (green and pink curves, respectively, bottom of graph; from Hogg et al. 2016a and the present study). The gray band highlights the collapse of the IHG between 12,960–12,840 cal BP, which corresponds to the rise of pCO₂ and the drastic drop of CH₄ at the onset of the Younger Dryas cold period.

of 56–58 yr for the SH calibration curve (SHCal04), with a variability of ±8 yr at 1000 cal BP and ±25 yr at 11,000 cal BP.

Hogg et al. (2016a) calculated the ¹⁴C-IHG for most of the YD event. They found variable values (averaged to 38 ± 6 yr), which are generally in agreement with the data for the last two millennia (44 ± 17 yr; Hogg et al. 2011). The same authors also described a collapse of the ¹⁴C-IHG during the period between 13,100 and 12,660 cal BP (Hogg et al. 2016a). However, annual-resolution ¹⁴C data from French trees spanning the early part of the YD around 12,660 cal BP indicate that the ¹⁴C-IHG was similar to the modeled value calculated by McCormac et al. (2004), with no evidence of a collapse (Capano et al. 2018).

For this study we can evaluate the ¹⁴C-IHG with the Barbiers record, extended to 415-yr with improved resolution with respect to our previous publication (Capano et al. 2018). To calculate the ¹⁴C-IHG, the Barbiers data from the NH were compared to the kauri data from the SH.

Table 2 Results of the comparison between the 10 averaged groups of Barbiers series and kauri record obtained by using OxCal program. IHG values in ^{14}C yr are obtained by using a uniform Delta_R function (U(-120,120)). Calibrated ranges refer to the first and last years of the chronology for each group.

Groups	Agreement % Acomb	IHG yr $\pm 2\sigma$ (modeled Delta_R)	Calibrated range (cal BP $\pm 2\sigma$)
1–10	432	40 \pm 6	13,012–12,597 \pm 5
2–11	433	40 \pm 6	13,002–12,588 \pm 5.5
3–12	429	40 \pm 7	13,003–12,588 \pm 6
4–13	435	37 \pm 7	13,001–12,586 \pm 6
5–14	457	37 \pm 6	13,001–12,586 \pm 5
6–15	463	37 \pm 6	13,001–12,586 \pm 6
7–16	439	37 \pm 6	13,010–12,596 \pm 4.5
8–17	440	38 \pm 6	13,011–12,596 \pm 4
9–18	431	39 \pm 6	13,012–12,597 \pm 4
10–19	430	40 \pm 6	13,013–12,598 \pm 4

As explained in the previous section dealing with chronological placement, Barbiers is averaged 10 times at decadal resolution and the ^{14}C -IHG calculation was performed at this same resolution, leading to 42–43 estimations, depending on the averaged curve. Considering the optimum correlation coefficient R for each of the 10 options, the ^{14}C -IHG was then calculated by subtracting the Barbiers ^{14}C age and $\Delta^{14}\text{C}$ ‰ from the corresponding kauri decadal ^{14}C -age and $\Delta^{14}\text{C}$ values ($\Delta t = (^{14}\text{C} \text{ age})_{\text{kauri}} - (^{14}\text{C} \text{ age})_{\text{Barb}}$, $\Delta \Delta^{14}\text{C} = \Delta^{14}\text{C}_{\text{kauri}} - \Delta^{14}\text{C}_{\text{Barb}}$). Note that the ratio between the ^{14}C -IHG in age and in ‰ is not strictly constant. This is due to the fact that both $\Delta^{14}\text{C}$ values are elevated and vary through time (N.B. if the $\Delta^{14}\text{C}$ values were close to 0, the Taylor series approximation of $\text{Ln}(1+x) = x$ at first order would lead to $\Delta t = -8 \cdot \Delta \Delta^{14}\text{C}$).

The ^{14}C -IHG shows mean values ranging between 31 yr with a SD of 23 yr and 43 yr with a SD of 23 yr, depending on the chronological placement (–5 to –7‰). Minimizing the χ^2 distance provides a direct estimation of the ^{14}C -IHG (Figure 4). Depending on the chronological placement, the optimum IHG value varies from 34 to 46 yr (–5 to –7‰). Matching the Barbiers and kauri decadal records with the Oxcal program, also provides a direct ^{14}C -IHG estimation, which ranges between 37 and 40 yr (–6‰; Table 2). Overall, the three statistical techniques provide similar ^{14}C -IHG values.

Considering only the best chronological placement, 13,008–12,594 ± 10 cal BP, the mean ^{14}C -IHG value is 37 yr with a SD of 21 yr ($n = 43$), –6‰ with a SD of 3‰ (Figure 3). The ^{14}C -IHG time variations in Figure 3 indicate two periods with minimal values close to 0 from 12,960 to 12,900 cal BP and from 12,860 to 12,840 cal BP, where the ^{14}C -IHG oscillates between –4 and 24 yr (between 1 and –4‰):

- During the first period (12,960–12,900 cal BP) the mean ^{14}C -IHG is 10 yr with a SD of 12 yr ($n = 7$), –2‰ with a SD of 2‰.
- During the second period (12,860–12,840 cal BP), the mean ^{14}C -IHG is 6 yr with a SD of 12 yr ($n = 3$), –1‰ with a SD of 2‰.

The period in-between (12,890–12,870 cal BP) shows a value of 39 yr with a SD of 4 yr ($n = 3$), -6‰ with a SD of 1‰ , in agreement with the overall mean ^{14}C -IHG of 37 yr.

These intervals with minimum ^{14}C -IHG correspond in time to the beginning of the YD event at $12,846 \pm 138$ cal BP (Rasmussen et al. 2006).

By excluding the two short periods with minimal ^{14}C -IHG, it is possible to recalculate a mean ^{14}C -IHG of 45 yr with a SD of 14 yr ($n = 33$), -7‰ with a SD of 2‰ . These values are indistinguishable from the ^{14}C -IHG observed over the last two millennia (44 yr with a SD of 17 yr; Hogg et al. 2011).

The plot of ^{14}C age versus calendar ages (Figures 1, 5) exhibits three “age plateaux” during the periods 13,010–12,970 cal BP, at the beginning of the Barbiere chronology, 12,820–12,770 cal BP, immediately before the drastic $\Delta^{14}\text{C}$ rise, and 12,720–12,690 cal BP, immediately after the $\Delta^{14}\text{C}$ rise. The ^{14}C -IHG determination is expected to be particularly robust during these periods. Indeed, a slight inaccuracy in the chronological placement of the Barbiere sequence with respect to the kauri record would not affect the ^{14}C difference over an “age plateau.” The IHG during the three “age plateaux” is the following:

- Over the 13,010–12,970 cal BP “plateau” the ^{14}C -IHG average is 37 yr with a SD of 14 yr (-6‰ with a SD of 2‰ ; $n = 5$).
- For the 12,820–12,770 cal BP “plateau” the ^{14}C -IHG average is 49 yr with a SD of 9 yr (-7‰ with a SD of 1‰ ; $n = 6$).
- During the 12,720–12,690 cal BP plateau the ^{14}C -IHG average is 53 yr with a SD of 9 yr (-8‰ with a SD of 1‰ ; $n = 4$).

During each of the three “plateaux,” the individual decadal ^{14}C -IHG values are fully compatible with each other. It is thus reasonable to assume that the ^{14}C -IHG was stable during these periods. Under this hypothesis, we can calculate one sigma errors of the mean ($\text{SE} = \text{SD}/\sqrt{n}$) for the ^{14}C -IHG determinations: 37 ± 6 yr, 49 ± 4 and 53 ± 5 yr, respectively for the three ^{14}C “age plateaux” in chronological order. The data suggest that the first ^{14}C -IHG value is thus statistically lower than the two other values. This may indicate that the IHG increased during the transition between the Allerød and the YD periods at around 12,846 cal BP, but, more ^{14}C data will obviously be needed to verify this suggestion. An additional problem is that the uncertainty on the climatic transition is large (± 138 yr in the Greenland ice GICC05 chronology). Identification of this transition directly in the trees would certainly help to resolve the issue.

The period between 12,760 and 12,730 cal BP is characterized by a drastic $\Delta^{14}\text{C}$ rise of 25‰ . However, the ^{14}C -IHG remains high, with a mean of 55 yr, and relatively stable, with a SD of 19 yr based on 4 values (-8‰ and a SD of 3‰). This translates to an ^{14}C -IHG estimate of 55 yr and SE of 10 yr, which agrees with the overall mean and SE of 45 ± 2 yr (excluding the two brief periods of minimal IHG).

The ^{14}C -IHG in subfossil trees reflects the asymmetry between the ^{14}C signatures of CO_2 fluxes to the atmosphere in the SH and NH. Variations of the ^{14}C -IHG are thus to be expected when the N-S balance of CO_2 fluxes is perturbed in both ocean and land sources. For example, Rodgers et al. (2011) used an ocean-atmosphere model to study the ^{14}C -IHG variations over the last millennium and attributed an abrupt ^{14}C -IHG decrease by 16 yr (2‰ in $\Delta^{14}\text{C}$) to a weakening of the Westerlies in the Southern Ocean.

The new ^{14}C record of Barbiers trees suggests a ^{14}C -IHG increase between the end of the Allerød (IHG = 37 ± 6 yr) and the early YD (IHG = 48 ± 3 yr). This is compatible with ocean circulation changes, namely: a decrease in deep-water convection in the North-Atlantic and an associated increase in wind-driven upwelling in the Southern Ocean.

The new ^{14}C -IHG record also shows a 120-yr period (12,960–12,840 cal BP) characterized by two brief phases of minimal values followed by the YD increase: the first of these phases lasted 6 decades, while the second was shorter, spanning 2 decades only. It is reasonable to hypothesize that these century-long anomalies in ^{14}C -IHG are in fact synchronous with the start of the YD event.

It is also important to note that the ^{14}C -IHG minima are also synchronous with $\Delta^{14}\text{C}$ minima in both the NH and SH. This suggests that this century-long period was characterized by a strong release of relatively old CO_2 , preferably into the NH atmosphere. The timing of the $\Delta^{14}\text{C}$ decrease would thus correspond to the start of the rise in atmospheric CO_2 that occurred at the beginning of the YD (Figure 6).

Further analyses are needed to confirm our observations, together with carbon cycle modeling to simulate the triple isotope signatures and the ^{14}C -IHG. Between 13,000 and 12,800 cal BP, atmospheric $\Delta^{14}\text{C}$ is rather stable, but exhibits century-long cycles with minima corresponding to the two ^{14}C -IHG anomalies. It will be important to evaluate the possible variations of the ^{14}C production during this period by comparing the observed $\Delta^{14}\text{C}$ variations with those in the ^{10}Be record from ice cores (e.g. Bard et al. 1997; Adolphi et al. 2018). Nevertheless, cosmogenic production changes through solar modulation should affect both hemispheres in a rather symmetric way. Hence, CO_2 fluxes in the NH from old carbon oxidation can be seen as a possible mechanism to explain the observed variations.

CONCLUSIONS

We have analyzed a 416-yr-long tree-ring chronology from subfossil trees (*Pinus sylvestris* L.) which grew in the southern French Alps during the Younger Dryas cold period. ^{14}C measurements at annual resolution of this Barbiers chronology were performed at least every third year of the sequence, establishing a high-resolution ^{14}C sequence in a period characterized by tree growth recession.

We date the new Barbiers record to 13,008–12,594 ± 10 cal BP by matching the ^{14}C patterns with those of the kauri chronology. Consequently, the Barbiers record should include the transition between the Allerød and YD events at 12,846 cal BP, although the exact position of the boundary is still uncertain due to the error of the ice core chronology (138 yr).

Our new data allow to calculate the ^{14}C -IHG between the Northern Hemisphere (Barbiers pines from France) and the Southern Hemisphere (kauri trees from New Zealand). The mean ^{14}C -IHG is 37 yr with a SD of 21 yr based on 43 decadal estimations.

Over the 415 yr, the ^{14}C -IHG exhibit minimal values of between 12,960–12,840 cal BP. Excluding these minima from the average, leads to a mean ^{14}C -IHG of 45 yr with a SD of 14 yr based on 33 decadal values, in agreement with observations for the last two millennia.

The Barbiers record suggests a ^{14}C -IHG increase between the end of the Allerød period (IHG = 37 ± 6 yr) and the early part of the YD (IHG = 48 ± 3 yr). This change is

compatible with a previously reported drop of deep-water convection in the North-Atlantic and an associated increase in wind-driven upwelling in the Southern Ocean.

Between 12,960 and 12,840 cal BP the ^{14}C -IHG minima are accompanied by $\Delta^{14}\text{C}$ minima in both the NH and SH. These data have been compared with the records of CO_2 and CH_4 mixing ratios measured in air bubbles occluded in Antarctic ice. The concomitant ^{14}C -IHG and $\Delta^{14}\text{C}$ minima seem to correspond to the start of the rise in atmospheric CO_2 and the decrease in CH_4 at the beginning of the YD.

Further work is needed using carbon cycle modeling to simulate the various carbon isotope signatures, so as to take into account possible variations of ^{14}C production during this period by considering variations in the ^{10}Be ice core record.

ACKNOWLEDGMENTS

AixMICADAS and its operation are funded by the Collège de France, the EQUIPEX ASTER-CEREGE and the ANR project CARBOTRYDH (PI E.B.).

SUPPLEMENTARY MATERIAL

To view supplementary material for this article, please visit <https://doi.org/10.1017/RDC.2019.116>

REFERENCES

- Adolphi F, Muscheler R, Friedrich M, Gütthler D, Wacker L, Talamo S, Kromer B. 2017. Radiocarbon calibration uncertainties during the last deglaciation: Insights from new floating tree-ring chronologies. *Quaternary Science Reviews* 170: 98–108.
- Adolphi F, Bronk Ramsey C, Erhardt T, Lawrence Edwards R, Cheng H, Turney CSM, Cooper A, Svensson A, Rasmussen SO, Fischer H, Muscheler R. 2018. Connecting the Greenland ice-core and U/Th timescales via cosmogenic radionuclides: Testing the synchronicity of Dansgaard-Oeschger events. *Climate of the Past Discussions* 14: 1755–1781.
- Bard E. 1988. Correction of accelerator mass spectrometry ^{14}C ages measured in planktonic foraminifera: Paleoceanographic implications. *Paleoceanography* 3:635–645.
- Bard E, Raisbeck G, Yiou F, Jouzel J. 1997. Solar modulation of cosmogenic nuclide production over the last millennium: comparison between ^{14}C and ^{10}Be records. *Earth and Planetary Science Letters* 150:453–462.
- Bard E, Tuna T, Fagault Y, Bonvalot L, Wacker L, Fahrni S, Synal H-A. 2015. AixMICADAS, the accelerator mass spectrometer dedicated to ^{14}C recently installed in Aix-en-Provence, France. *Nuclear Instruments and Methods in Physics Research B* 361:80–86.
- Braziunas TF, Fung IY, Stuiver M. 1995. The pre-industrial atmospheric $^{14}\text{CO}_2$ latitudinal gradient as related to exchanges among atmospheric oceanic and terrestrial reservoirs. *Global Biogeochemical Cycles* 9:565–584.
- Bronk Ramsey C, van der Plicht J, Weninger B. 2001. “Wiggle matching” radiocarbon dates. *Radiocarbon* 43(2):381–389.
- Bronk Ramsey C. 2009. Dealing with outliers and offsets in radiocarbon dating. *Radiocarbon* 51(3): 1023–1045.
- Bronk Ramsey C, Staff RA, Bryant CL, Brock F, Kitagawa H, van der Plicht J, Scholaut G, Marshall MH, Brauer A, Lamb HF, Payne RL, Tarasov PE, Haraguchi T, Gotanda K, Yonenobu H, Yokoyama Y, Tada R, Nakagawa T. 2012. A complete terrestrial radiocarbon record for 11.2 to 52.8 kyr B.P. *Science* 338: 370–374.
- Buizert C, Cuffey KM, Severinghaus JP, Baggenstos D, Fudge TJ, Steig EJ, Markle BR, Winstrup M, Rhodes RH, Brook EJ, Sowers TA, Clow GD, Cheng H, Edwards RL, Sigl M, McConnell JR, Taylor KC. 2015. The WAIS Divide deep ice core WD2014 chronology. Part 1: Methane synchronization (68–31 ka BP) and the gas age-ice age difference. *Climate of the Past* 11:153–173.
- Capano M, Miramont C, Guibal F, Kromer B, Tuna T, Fagault Y, Bard E. 2018. Wood ^{14}C dating with AixMICADAS: methods and application to tree-ring sequences from the Younger Dryas event in the southern French Alps. *Radiocarbon* 60(1):51–74.
- Cook ER, Kairiukstis LA. 1990. Methods of dendrochronology. Applications in the environmental

- sciences. International Institute for Applied Systems Analysis. Dordrecht: Kluwer Academic Publishers. 394 p.
- Frei C, Schär C. 1998. A precipitation climatology of the Alps from high-resolution rain-gauge observations. *International Journal of Climatology* 18:873–900.
- Friedrich M, Remmele S, Kromer B, Hofmann J, Spurk M, Kauser KF, Orsel C, Kuppers M. 2004. The 12,460-year Hohenheim oak and pine tree-ring chronology from Central Europe; a unique annual record for radiocarbon calibration and paleoenvironment reconstructions. *Radiocarbon* 46(3):1111–1122.
- Fritts HC. 1976. *Tree rings and climate*. New York: Academic Press. 567 p.
- Gidon M, Montjuvent G, Flandrin J, Moullade M, Durozoy G, Damiani L. 1991. Carte géologique au 50/000, Laragne, BRGM edition.
- Hogg AG, McCormac FG, Higham TFG, Reimer PJ, Baillie MGL, Palmer JG. 2002. High-precision radiocarbon measurements of contemporaneous tree-ring dated wood from the British Isles and New Zealand: AD 1850-950. *Radiocarbon* 44(3): 633–640.
- Hogg A, Palmer J, Boswijk G, Chris, Turney C. 2011. High-precision radiocarbon measurements of tree-ring dated wood from New Zealand: 195 BC–AD 995. *Radiocarbon* 53(3):529–542.
- Hogg A, Turney C, Palmer J, Southon J, Kromer B, Bronk Ramsey C, Boswijk G, Fenwick P, Noronha A, Staff R, Friedrich M, Reynard L, Guettler D, Wacker L, Jones R. 2013. The New Zealand kauri (*Agathis australis*) research project: A radiocarbon dating intercomparison of Younger Dryas wood and implications for IntCal13. *Radiocarbon* 55(4):2035–2048.
- Hogg A, Southon J, Turney C, Palmer J, Bronk Ramsey C, Fenwick P, Boswijk G, Friedrich M, Helle G, Hughen K, Jones R, Kromer B, Noronha A, Reynard L, Staff R, Wacker L. 2016a. Punctuated shutdown of Atlantic meridional overturning circulation during Greenland Stadial 1. *Nature-Scientific Report* 6:25902.
- Hogg A, Southon J, Turney C, Palmer J, Bronk Ramsey C, Fenwick P, Boswijk G, Buüntgen U, Friedrich M, Helle G, Hughen K, Jones R, Kromer B, Noronha A, Reinig F, Reynard L, Staff R, Wacker L. 2016b. Decadally resolved lateglacial radiocarbon evidence from New Zealand kauri. *Radiocarbon* 58(4):709–733.
- Hua Q, Barbetti M, Fink D, Kaiser KF, Friedrich M, Kromer B, Levchenko VA, Zoppi U, Smith AM, Bertuch F. 2009. Atmospheric ^{14}C variations derived from tree rings during the early Younger Dryas. *Quaternary Science Reviews* 28(25–26): 2982–2990.
- Hughen K, Southon J, Lehman S, Overpeck T. 2000. Synchronous radiocarbon and climate shifts during the last deglaciation. *Science* 290: 1951–1954.
- Jorda M, Rosique T, Évin J. 2000. Données nouvelles sur l'âge du dernier maximum glaciaire dans les Alpes méridionales françaises. *Comptes Rendus de l'Académie des Sciences. Série 2, Sciences de la Terre et des Planètes* 331(3):187–193.
- Kaiser KF, Friedrich M, Miramont C, Kromer B, Sgier M, Schaub M, Boeren I, Remmele S, Talamo S, Guibal F, Sivan O. 2012. Challenging process to make the Lateglacial tree-ring chronologies from Europe absolute. *Quaternary Science Reviews* 36:78–90.
- Kieffer-Weisse A, Bois P. 2001. Estimation de paramètres statistiques des précipitations extrêmes dans les Alpes françaises, *La Houille Blanche* (1): 62–70.
- Kromer B, Friedrich M, Talamo S. 2015. Progress report on dendrochronology and 14C of the Hohenheim Preboreal/YD and Late Glacial pine chronologies. Oral presentation at Zürich IntCal-Dendro Meeting (Zürich, 4–5 August 2015).
- Lerman JC, Mook WG, Vogel JC. 1970. C14 in tree rings from different localities. In: Olsson IU, editor. *Radiocarbon Variations and Absolute Chronology*. New York: John Wiley: 275–300.
- Levin I, Kromer B, Wagenbach D, Munnich KO. 1987. Carbon isotope measurements of atmospheric CO_2 at a coastal station in Antarctica. *Tellus* 39B(1–2): 89–95.
- Libby WF. 1954. Chicago radiocarbon dates V. *Science* 120(3123):733–742.
- Marcott SA, Bauska TK, Buizert C, Steig EJ, Rosen JL, Cuffey KM, Fudge TJ, Severinghaus JP, Ahn J, Kalk ML, McConnell JR, Sowers T, Taylor KC, White JWC, Brook EJ. 2014. Centennial-scale changes in the global carbon cycle during the last deglaciation. *Nature* 514:616–619.
- McCormac FG, Hogg AG, Higham TG, Baillie ML, Palmer JG, Xiong L, Pilcher JR, Brown D, Hoper ST. 1998. Variations of radiocarbon in tree rings: Southern Hemisphere offset preliminary results. *Radiocarbon* 40(3):1–7.
- McCormac FG, Hogg AG, Blackwell PG, Buck CE, Higham TFG, Reimer PJ. 2004. SHCAL04 Southern Hemisphere calibration, 0–11.0 cal. kyr BP. *Radiocarbon* 46(3):1087–1092.
- Miramont C, Sivan O, Rosique T, Edouard JL, Jorda M. 2000. Subfossil tree deposits in the middle Durance (Southern Alps, France); environmental changes from Allerød to Atlantic. *Radiocarbon* 42(3):423–435.
- Miramont C, Rosique T, Sivan O, Edouard JL, Magnin F, Talon B. 2004. Le cycle de sédimentation « postglaciaire principal » des bassins marneux sub-alpins : état des lieux. *Méditerranée* 1(2):71–84.
- Miramont C, Guibal F, Kaiser KF, Kromer B, Sgier M, Sivan O, Friedrich M, Talamo S. 2010. L'apport des séries dendrochronologiques françaises au prolongement de la chronologie européenne absolue et à la calibration du

- radiocarbone. In Cahiers de Géographie 11, Collection EDYTEM: 189–198.
- Miramont C, Sivan O, Guibal F, Kromer B, Talamo S, Kaiser KF. 2011. L'étalonnage du temps du radiocarbon par les cernes d'arbre. L'apport des series dendrochronologiques du gisement de bois subfossiles du torrent des Barbiers (Alpes Françaises du sud). *Quaternaire* 22(3):261–271.
- Muscheler R, Kromer B, Björck S, Svensson A, Friedrich M, Kaiser KF, Southon J. 2008. Tree rings and ice cores reveal ^{14}C calibration uncertainties during the Younger Dryas. *Nature Geoscience* 1: 263–267.
- Rasmussen SO, Andersen KK, Svensson AM, Steffensen JP, Vinther BM, Clausen HB, Siggaard-Andersen ML, Johnsen SJ, Larsen LB, Dahl-Jensen D, Bigler M, Röthlisberger R, Fischer H, Goto-Azuma K, Hansson ME, Ruth U. 2006. A new Greenland ice core chronology for the last glacial termination. *Journal of Geophysical Research* 111:D06102.
- Reimer PJ, Bard E, Bayliss A, Beck JW, Blackwell PG, Bronk Ramsey C, Buck CE, Cheng H, Edwards RL, Friedrich M, Grootes PM, Guilderson TP, Hafflidason H, Hajdas I, Hatté C, Heaton TJ, Hoffmann DL, Hogg AG, Hughen KA, Kaiser KF, Kromer B, Manning SW, Niu M, Reimer RW, Richards DA, Scott EM, Southon JR, Staff RA, Turney CSM, van der Plicht J. 2013. IntCal13 and Marine13 radiocarbon age calibration curves 0–50,000 years cal BP. *Radiocarbon* 55(4):1869–1887.
- Reinig F, Nievergelt D, Esper J, Friedrich M, Helle G, Hellmann L, Kromer B, Morganti S, Pauly M, Sookdeo A, Tegel W, Treydte K, Verstege A, Wacker L, Büntgen U. 2018. New tree-ring evidence for the Late Glacial period from the northern pre-Alps in eastern Switzerland. *Quaternary Science Reviews* 186:215–224.
- Rinn F. 1996. TSAP e, time series analyses presentation. Version 3.0. Reference manual. Heidelberg. 262 p.
- Rinn F. 2003. TSAP-Win, time series analysis and presentation for dendrochronology and related applications. Version 0.53. Reference manual. Heidelberg: Rinn Tech.
- Rodgers KB, Mikaloff-Fletcher SE, Bianchi D, Beaulieu C, Galbraith ED, Gnanadesikan A, Hogg AG, Iudicone D, Lintner BR, Naegler T, Reimer PJ, Sarmiento JL, Slater RD. 2011. Interhemispheric gradient of atmospheric radiocarbon reveals natural variability of Southern Ocean winds. *Climate of the Past* 7:1123–1138.
- Schaub M, Kaiser KF, Frank DC, Buentgen U, Kromer B, Talamo S. 2008. Environmental change during the Allerød and Younger Dryas reconstructed from tree-ring data. *Boreas* 37:74–86.
- Sivan O, Miramont C, Edouard JL. 2006. Rythmes de la sédimentation et interprétations paléoclimatiques lors du Postglaciaire dans les Alpes du Sud. ^{14}C et dendro-géomorphologie, deux chronomètres complémentaires. In: Allée P, Lespez L, directors. L'Érosion entre Société, Climat et Paléoenvironnement. Table ronde en l'honneur du Professeur René Neboit-Guilhot. Clermont-Ferrand, 25–27 March 2004: 423–428.
- Sookdeo A, Wacker L, Adolphi F, Beer J, Büntgen U, Friedrich M, Helle G, Hogg A, Kromer B, Muscheler R, Nievergelt D, Palmer J, Pauly M, Reinig F, Turney C, Synal H-A. 2019. Quality dating: A well-defined protocol for quality high-precision ^{14}C -dates tested on Late Glacial wood. *Radiocarbon* 61(6). In press.
- Stuiver M, Polach HA. 1977. Discussion: reporting of ^{14}C data. *Radiocarbon* 19(3):355–363.
- Stuiver M, Braziunas T. 1998. Anthropogenic and solar component of hemispheric ^{14}C . *Geophysical Research Letters* 25(3):329–332.
- Wacker L, Bayliss A, Brown D, Friedrich M, Scott M. 2018. First radiocarbon inter-comparison on annual tree-ring samples. Poster presentation at 23rd International Radiocarbon Conference, Trondheim, Norway, 17–22 June 2018.